CLS
COLLECTE LOCALISATION SATELLITES

Consortium Members

TU Delft Delft University of Technology | SATOC Satellite Oceanographic Consultants | DTU Space National Space Institute | isardSAT | National Oceanography Centre Natural Environment Research Council | NOVELTIS | Starlab Living Science | U.PORTO Faculdade de Ciências Universidade do Porto

ESA Cryosat Plus for Oceans

Product Validation Report (PVR) of the CPP RDSAR processing for oceans

Reference:	CLS-DOS-NT-13-155
Nomenclature:	CP4O-PVR-XXX
Issue:	1. 0
Date:	Jun. 18, 13

esa European Space Agency

cnes CENTRE NATIONAL D'ÉTUDES SPATIALES

Chronology Issues:			
Issue:	Date:	Reason for change:	Author
1.0	18/06/13	Creation of PVR Issue 1.0	T. Moreau F. Boy M. Raynal

People involved in this issue:		
Written by (*):	T. Moreau (CLS) F. Boy (CNES) M. Raynal (CLS)	Date + Initials:(visa or ref)
Checked by (*):	S. Labroue (CLS)	Date + Initial:(visa ou ref)
Approved by (*):	P. Thibaut (CLS)	Date + Initial:(visa ou ref)
Application authorized by (*):	XXX (ESA) N. Picot (CNES)	Date + Initial:(visa ou ref)

**In the opposite box: Last and First name of the person + company if different from CLS*

Index Sheet:	
Context:	
Keywords:	[Mots clés]
Hyperlink:	

Distribution:		
Company	Means of distribution	Names
CLS	Notification	

List of tables and figures

List of tables:

Aucune entrée de table d'illustration n'a été trouvée.

List of figures:

Applicable documents

Reference documents

RD 1 Manuel du processus Documentation
CLS-DOC

RD 2 Algorithm Theoretical Basis Document (ATBD) of the CPP RDSAR processing for oceans
S3A-NT-SRAL-00098-CNES

Acronyms List

AIR	Azimuth Impulse Response
ATBD	Algorithm Theoretical Basis Document
BRF	Burst Repetition Frequency
CPP	Cryosat Processing Prototype
DUACS	Data Unification and Altimeter Combination System
EO	Earth Observation
FBR	Full Bit Rate (un-calibrated, geo-located I and Q individual echoes in time domain)
FSSR	Flat Sea Surface Response
LRM	Low Resolution Mode
LSE	Least Squares Estimator
NA	Not Applicable
NRT	Near Real Time
POD	Precise Orbit Determination
PTR	Point Target Response
PVR	Plan Validation Report
RD	Reference Document
RDSAR	Reduces Synthetic Aperture radar
RIR	Range Impulse Response
SAR	Synthetic Aperture radar
SIRAL	Synthetic Aperture Interferometric Radar Altimeter
SLA	Sea level Anomalies
SSB	Sea State Bias
SWH	Significant Wave Height

List of Contents

1. Introduction

1.1. Purpose and scope

This document is the Plan Validation Report (PVR) for the CryoSat-2 RDSAR L2 products over ocean, which is generated from the Cryosat Processing Prototype (CPP) by CNES. This document reports the validation results and error analyses of the CPP RDSAR L2 products, including a continuity assessment with respect to the CryoSat-2 LRM mode and cross-comparisons with measurements from other Earth Observation (EO) source.

1.2. Document structure

In the equatorial Pacific Ocean acquisition are performed in SAR mode. In this document we validate the CPP RDSAR derived SLA, SWH, Sigma-0 and mispointing angle at the LRM/SAR transition zone over this region (to assess biases).

In Section 2 we describe the data used. In Section 3 the validation of the CPP RDSAR L2 altimetric products is made by comparison to the CryoSat-2 LRM data (to ensure data quality continuity between SAR and LRM) and to EO satellite data (over the same time period that is considered). In Section 4 we discuss our results and provide an outlook for future investigations.

2. Data and method overview

2.1. Selection of the test area

Since the CryoSat-2 acquisition mode mask has been changed on May 7th 2012 (see Figure 2.1), there is currently one large area operated in SAR mode, located in equatorial Pacific Ocean, which is particularly adapted for SAR mode data validating purposes. This zone was defined based on the following criteria:

1. low ocean variability (so easing the inter-mission calibration with conventional altimetry satellites like Jason 2 and in preparation to Sentinel-3),
2. few occurrences of rain and sigma0 blooms events (which could have different impacts on SAR and RDSAR),
3. mean SWH around 2 meters and mean wind around 7 meters (so the sea state is close to the mean conditions).

This area is also of great interest for detecting ocean bathymetry features at high spatial resolution, in particular sea mounds mapping.

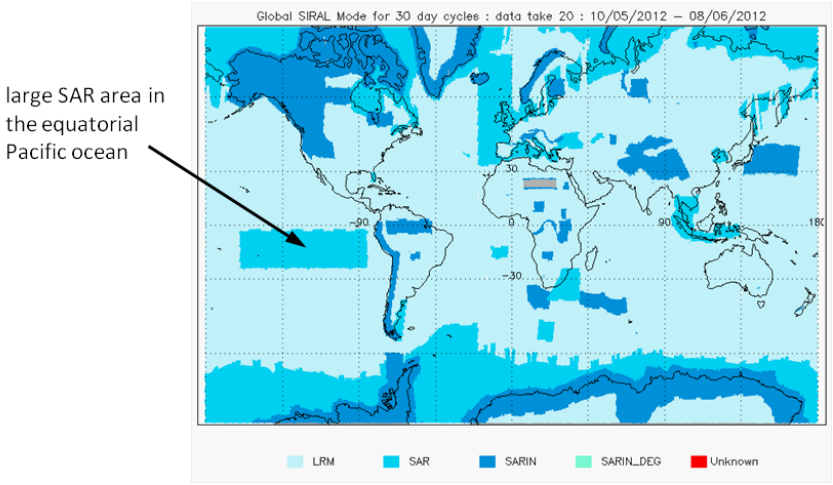

Figure 2.1: The mode mask, uploaded to CryoSat-2 in May 2012 (i.e. on May 7th).

2.2. Data used

2.2.1. Altimeter data

The RDSAR products are generated by the CPP chain processing according to the V13 RDSAR algorithm (see related ATBD document).

For this validation exercise, different types of data analysis will be performed:

- we will use a small set of measurements taken along the track (cycle 30, pass 82) spanning the period from 9:55 a.m. to 10:45 a.m. on May 7th 2012 (as shown in Figure 2.2). Only measurements located at positions in the equatorial Pacific ocean are selected, for latitude varying from +0° to -30° (in and outside the SAR-mode box). These data will be used to compare the CPP RDSAR products from one side of the LRM/SAR mode transition to the CPP LRM mode estimates on the other side.

- Secondly, we will use a whole cycle of data from May 2012. Retracked data using the CPP RDSAR method will be compared to the CPP LRM products and to the MLE4 retracked data found in the current SGDR Jason-2 products.

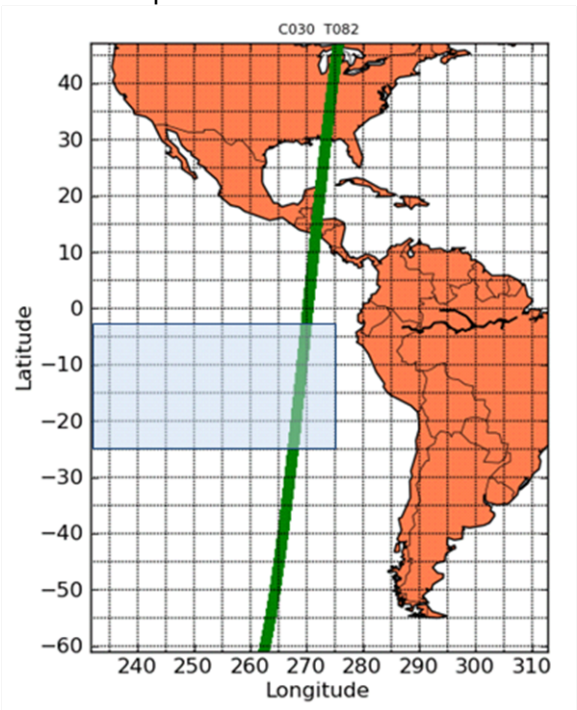

Figure 2.2: Segment of the track used (cycle 30, pass 82).

2.2.2. Selecting valid data

To analyze the consistency between RDSAR and LRM data in open ocean, only valid ocean data are selected. Specific editing criteria are applied:

- a valid flag is used, based on the validation task of CryoSat-2 performed by the CLS Space Oceanography Division. LRM estimates and on-board retracked data in SAR-mode are used for this purpose.
- Some data points that are validated through the preceding step may still exhibit inconsistent behavior (particularly for RDSAR products that have not been appropriately validated). SLA data higher than 1.5m above the reference level in both modes are filtered out to eliminate those outliers (that may be related to some spurious observations caused by rain and blooms, or others events).

2.2.3. Correcting estimates through LUT

Retracked ranges and SWHs have been corrected applying a correction Lookup Table inherited from Jason-2, to account for the Gaussian approximation of the Point Target Response (PTR) in the conventional Brown ocean retracker used for both modes. The range look-up correction could be assimilated to a bias lower than 2 cm, whereas the significant wave height look-up correction is dependent on waves (as high as 20cm) as shown in Figure 2.3.

In turn, the correction on the sigma0 is of the order of a few hundredths of a dB; it is neglected in regard to the overall error budget on this parameter.

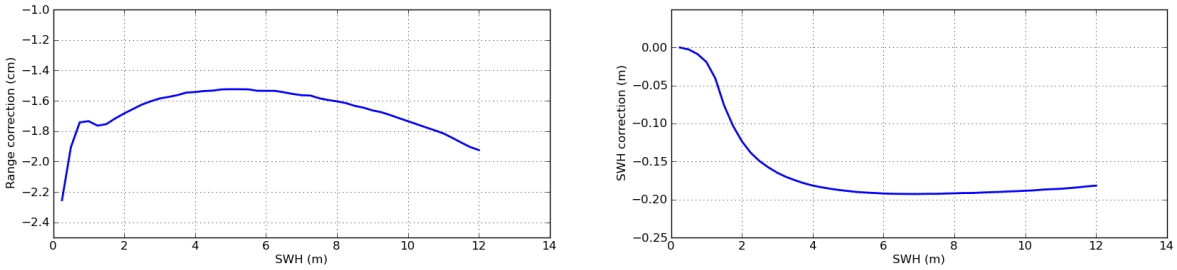

Figure 2.3: Range and SWH look-up table used for CPP products (corrections are in cm and m respectively).

An investigation is currently underway to update the correction LUT taking into account not only the approximation of the PTR in the retracking algorithm but also the characteristics of the CryoSat-2 altimeter (notably the ellipticity of the antenna) and the particular speckle reduction property of the RDSAR method (different from conventional altimetry mode).

2.2.4. Computing the sea level anomalies

Sea Level Anomalies (SLA) are computed by applying to the uncorrected sea level height the corrections available in the CPP products. The corrected sea level is defined as following for both datasets (LRM and RDSAR data):

$$SLA = Orbit - Range - i=0NCi - MSS + bias$$

where the *bias* allows to refer the CryoSat-2 data to the Jason-2 reference level (and to take care of the systematic bias between LRM CryoSat-2 and Jason-2 measurements), *Orbit* corresponds to the distance between the satellite and the ellipsoid, *Range* is the distance measured by the altimeter between the satellite and the sea surface, MSS is the Mean Sea Surface of the ocean over a long period and $i=0NCi$ is the sum of all the corrections needed to take into account the atmospherically effects (wet and dry troposphere, ionosphere, inverse barometer) and the geophysical phenomena (ocean tides, high frequency atmospheric effects on ocean). The various dynamic auxiliary data that are needed to process these altimeter data are displayed in Table 1.

Note that the sea-surface bias (electromagnetic sea-surface bias) has not been considered in the corrections for both cases since the SSB solution has not been calculated yet. In this way we use the same corrections for RDSAR and LRM sea level measurements.

Also note that a -1 ms datation bias is observed on LRM CryoSat-2 data, which is corrected in computing the SLA.

Orbit	Altitude of satellite above the reference ellipsoid - Cnes POE
Dry troposphere	Model dry tropospheric correction is computed at the altimeter time-tag from the interpolation of 2 meteorological fields that surround the altimeter time-tag. A dry tropospheric correction must be added (negative value) to the instrument range to correct this range measurement for dry tropospheric range delays of the radar pulse. From European Center for Medium Range Weather Forecasting
Wet troposphere	Model wet tropospheric correction is computed at the altimeter time-tag from the interpolation of 2 meteorological fields that surround the altimeter time-tag. A wet tropospheric correction must be added (negative value) to the instrument range to correct this range measurement for wet tropospheric range delays of the radar pulse. From European Center for Medium Range Weather Forecasting
Ionosphere	GIM ionospheric correction from NASA/JPL An ionospheric correction must be added (negative value) to the instrument range to correct this range measurement for ionospheric range delays of the radar pulse.
Ocean tide and loading tide	Geocentric ocean tide height (solution 1): GOT4.8 from GSFC Includes the loading tide and equilibrium long-period ocean tide height. The permanent tide (zero frequency) is not included in this parameter because it is included in the geoid and mean sea surface.
Solid Earth tide	Solid earth tide height is calculated using Cartwright and Taylor tables and consisting of the second and third degree constituents. The permanent tide (zero frequency) is not included. From Cartwright and Edden [1973] Corrected tables of tidal harmonics - J. Geophys. J. R. Astr. Soc., 33, 253-264.
Pole tide	Computed from Wahr [1985] Deformation of the Earth induced by polar motion - J. Geophys. Res. (Solid Earth), 90, 9363-9368.
Combined atmospheric correction	Also known as high frequency fluctuations of the sea surface topography which contains the combined atmospheric corrections (from MOG2D model + inverse barometer)
Mean Sea Surface	MSS_CNES_CLS-2011: mean sea surface height above reference ellipsoid from CLS/CNES

Table 1: Products corrections overview for Jason-2 and CryoSat-2.

3. Validation results and overall assessment

The overall objective of this validation exercise is to ensure that the CPP reduced SAR L2 products are fully consistent and valuable for maintaining the data quality continuity between SAR and LRM modes. This condition must be satisfied for enabling RDSAR data to be considered as a LRM reference during SAR mode.

In the following, the validation of this RDSAR algorithm (as described in the ATBD document) is performed with:

- the current CPP CryoSat-2 LRM (that is routinely assimilated in the DUACS multimission altimeter products). Comparisons of the SLA, SWH, Sigma-0, mispointing estimates in a SAR/LRM mode transition region, are performed.
- other satellite data. Comparisons of the SLA, SWH, sigma0 estimates using LRM data from the Jason-2 Poseidon-3 altimeter are performed over the same area.

3.1. Products along a single pass

Figure 3.1 shows the 1 Hz CPP products plotted along the pass 82 of cycle 30, in the equatorial Pacific area, for LRM and reduced SAR modes (as the pass is descending, this figure has to be read from right to left following decreasing latitudes). The SLA, SWH, backscatter coefficient (Sigma0) and mispointing estimates are obtained in both cases with the same ocean retracker (MLE-4 algorithm using a second order model [Amarouche et al., 2004]), but from different waveform processing algorithm (the traditional low resolution mode processing and CPP RDSAR respectively).

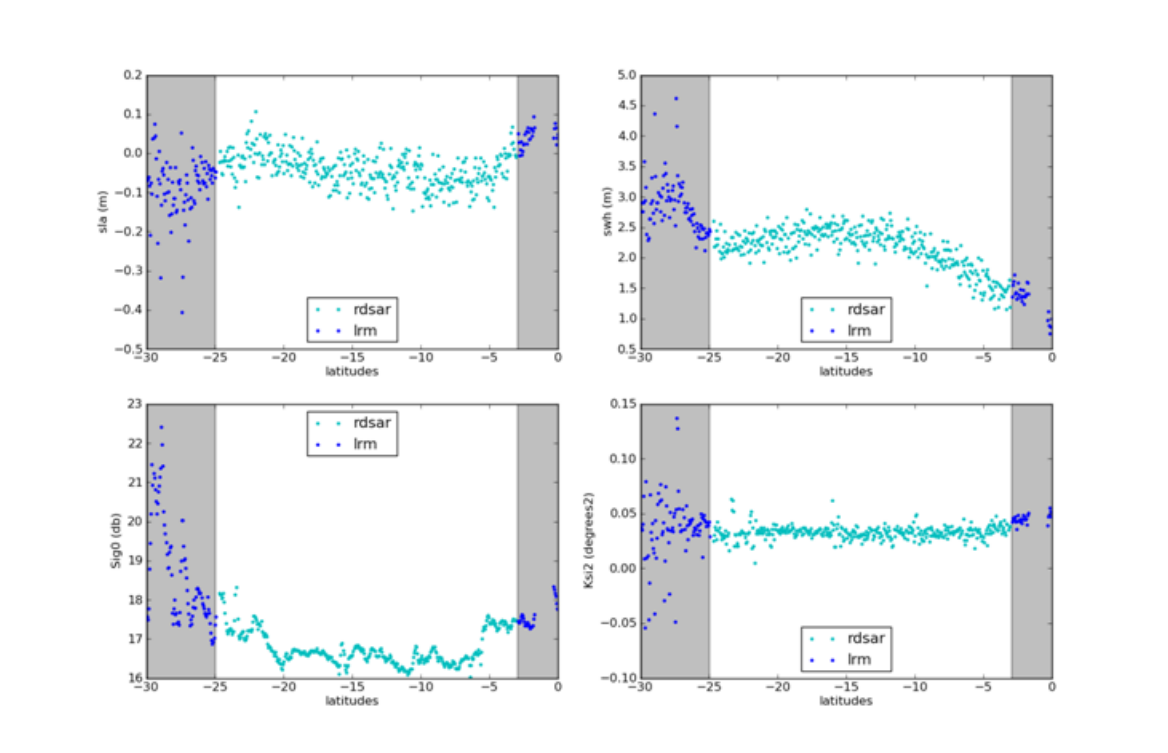

Figure 3.1: Sea Level Anomalies (upper left), significant wave height (upper right), Sigma0 coefficient (lower left) and mispointing angle (lower right) at 1 Hz in LRM mode (shaded area) and SAR mode (RDSAR) - Cycle 30 - pass 82.

We observe a quite good continuity and similar trend between LRM and RDSAR data on both sides of the transition zone. It is also important to note that the sigma0 coefficients have been shifted to be globally but roughly consistent with Jason-2 results. A precise evaluation of the bias will be performed, based on a more significant amount of data.

Figure 3.2 gives the corresponding 1 Hz noises on these parameters along the CryoSat-2 pass 82 of the cycle 30. We can see that the RDSAR parameter data are noisier that the LRM parameter data are. It is expected to be sqrt(90/32) times noisier. Figure 3.3 shows the performance curves of 1 Hz range (1 Hz range standard deviation vs. SWH) and 1 Hz SWH (1 Hz SWH standard deviation vs. SWH) for LRM and RDSAR data taken from several passes of cycle 30 crossing the test area. For SWH of 2 m the precision of 1 Hz range is 6.6 cm in LRM and 10.4 cm in RDSAR. Similarly, the precision of 1 Hz SWH is 44 cm in LRM and 64 cm in RDSAR.

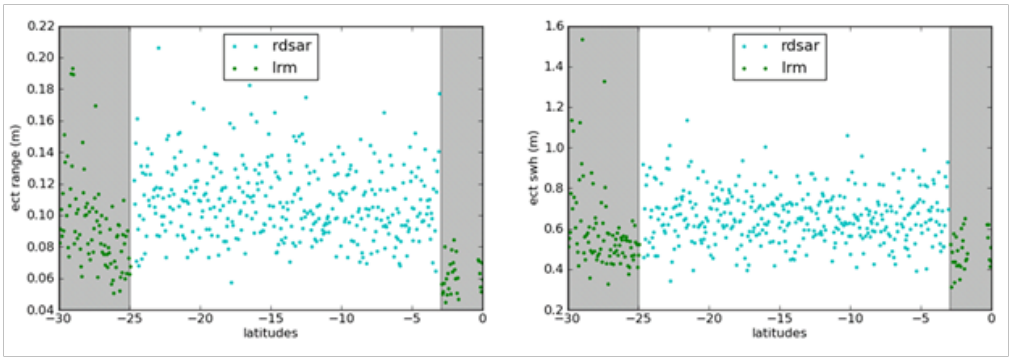

Figure 3.2: Precision of SLA (left), SWH (right) in LRM mode (shaded area) and SAR mode (RDSAR) along the pass 82 Cycle 30.

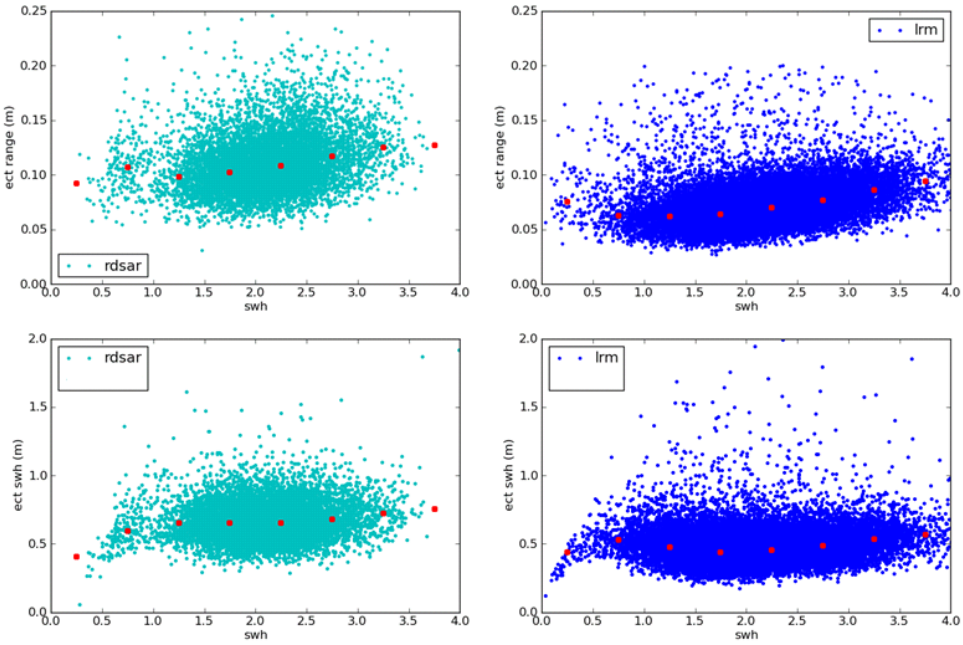

Figure 3.3: Precision of SLA (top) and SWH (bottom) in LRM mode (right) and SAR mode (left) from several passes of Cycle 30.

3.2. Validation of RDSAR product based on one cycle of data

This section shows a validation of these results based on a larger amount of data (a full cycle of data – cycle 30).

3.2.1. Map of estimates

Maps of LRM and RDSAR products in the equatorial Pacific test area are plotted in Figure 3.4. They are calculated globally (without separating ascending and descending passes). We can see a very good general agreement between LRM and RDSAR data over the region and notably at the transition between modes. Reduced SAR retrieval results are found to be very consistent with the ocean structure as observed by the LRM. To a lesser extent, only slight differences in mispointing angle are visible.

Beyond the good results achieved, we further examine the transition in the next section.

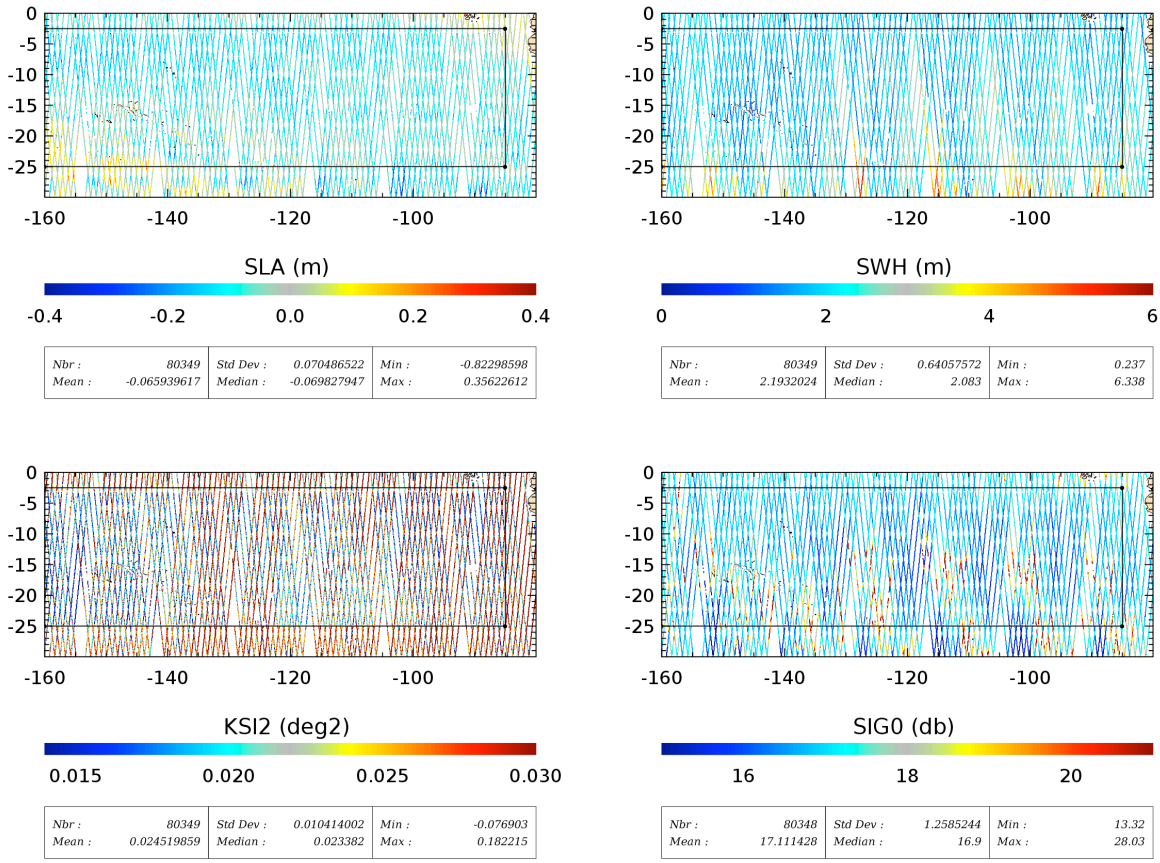

Figure 3.4: Maps of SLA (upper left), SWH (upper right), mispointing angles (lower left) and Sigma0 (lower right) values at 1 Hz in LRM mode and SAR mode (RDSAR) – Cycle 30. The contour line of the SAR mode area is drawn.

3.2.2. Assessment of the LRM data continuity

The mean of the SLA, SWH, Sigma-0 and mispointing angle is plotted with respect to latitude in Figure 3.5 to Figure 3.7. Each parameter is averaged per band of latitude of approximately 0.07° and for longitudes from 160° to 85° west (corresponding to the length of the SAR-mode Pacific ocean area). Various integration periods are examined: one cycle (Figure 3.5), 10 days (Figure 3.6) and 5 days (Figure 3.7).

In these plots, we can see an overall quite good agreement in SLA and SWH between LRM data from CryoSat-2 and Jason-2 missions. The similarity seems better for longer time period where the mean sea states have much better homogeneity in both cases. It is important to recall that Jason-2 and CryoSat-2 are flying on different ground track, so observing different scenes.

At the continuity, looking at the Figure 3.5 to Figure 3.7, it appears sudden spikes of values at the transition of both modes, such as a sharp drop or rise in SWH and SLA values over very short distance (tens of kms). These spikes are associated to the decrease of the number of data points accumulated per band of latitude as shown in Figure 3.8, corresponding likely to the presence of gaps in LRM and RDSAR data that may distort the mean per band.

In the south transition zone, as long as those spikes are not considered, the agreement between LRM and RDSAR SLA/SWH data is very good. It remains a little bias of 1 cm in SLA and a bias of few cm in wave height that may be explained by the use of no optimised look-up correction tables in the processing (indeed the RDSAR speckle reduction that is different from conventional altimetry mode is not taken into account in the LUT at this stage). This point needs to be verified.

At higher latitude of the test area (in the north transition zone), it is not easy to conclude about the continuity since a strong oceanic signal is located in the region (that is observed as a high gradient of SLA by Jason-2) that may dominate the errors.

On the other hand, these figures show that the agreement for the sigma0 coefficient is not as good as the other parameters. Discrepancies in sigma0 coefficients between LRM and RDSAR data is attributed to a bias caused. This bias is a typical consequence of an erroneous referencing (due to a rough and imprecise shift between both modes). This issue will be addressed and improved in future versions of the CPP products.

Additionally, a rupture of 0.06° occurs between the mispointing angles obtained from the LRM mode and RDSAR retracker (for a same platform). This bias may correspond to the error found of estimation of the mispointing angle with respect to simulated mispointing values due to noisier RDSAR waveforms. On-going investigations aim at computing an appropriate LUT to correct the CPP RDSAR data and so resolving this no significant discrepancy.

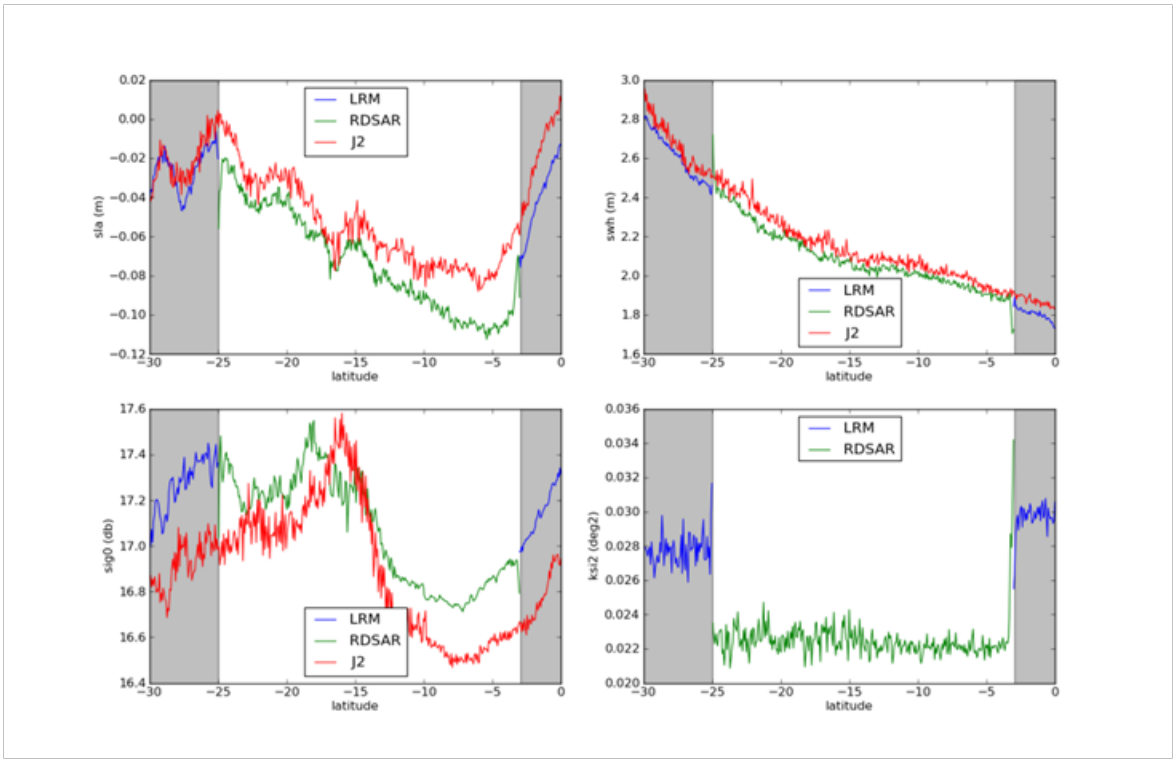

Figure 3.5: Mean of SLA (upper left), SWH (upper right), Sigma0 (lower left) and mispointing angles (lower right) by band of latitude for LRM and RDSAR of CryoSat-2 and LRM ofJason-2 – Cycle 30 – pass 82. The dashed zone corresponds to the LRM mode area.

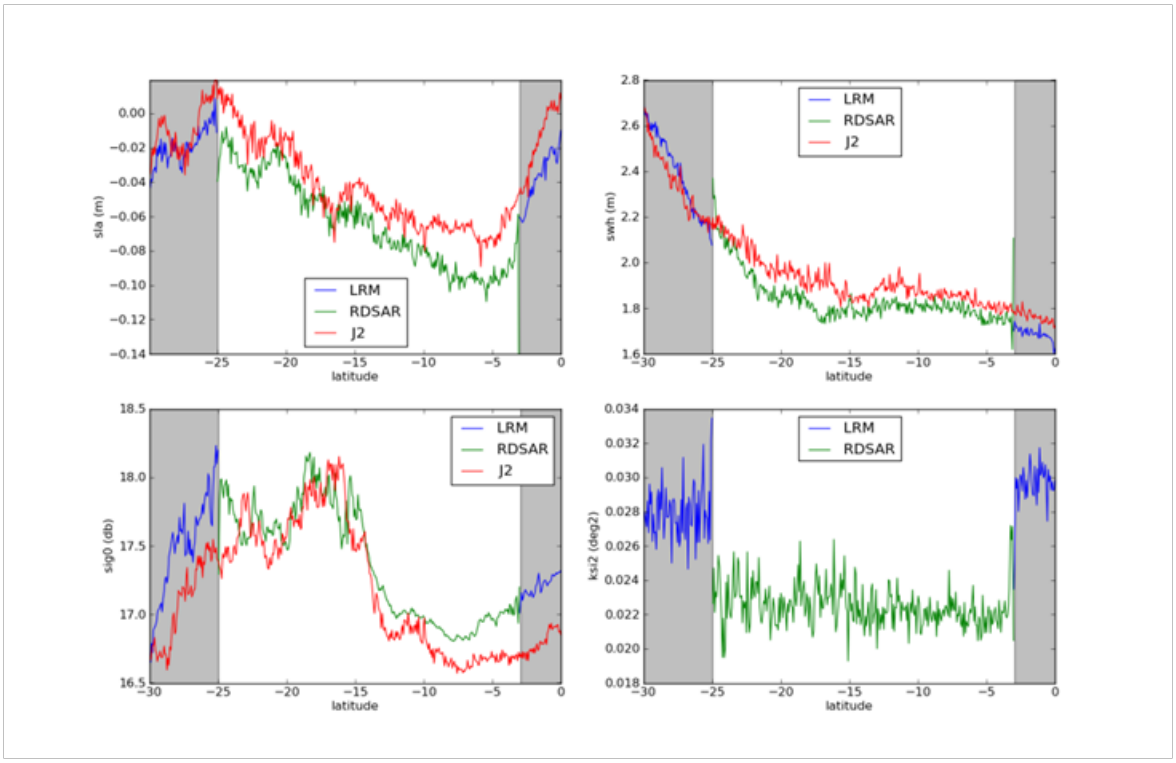

Figure 3.6: Mean of SLA (upper left), SWH (upper right), Sigma0 (lower left) and mispointing angles (lower right) by band of latitude for LRM and RDSAR of CryoSat-2 and LRM ofJason-2 – from 15th to 25th of May. The dashed zone corresponds to the LRM mode area.

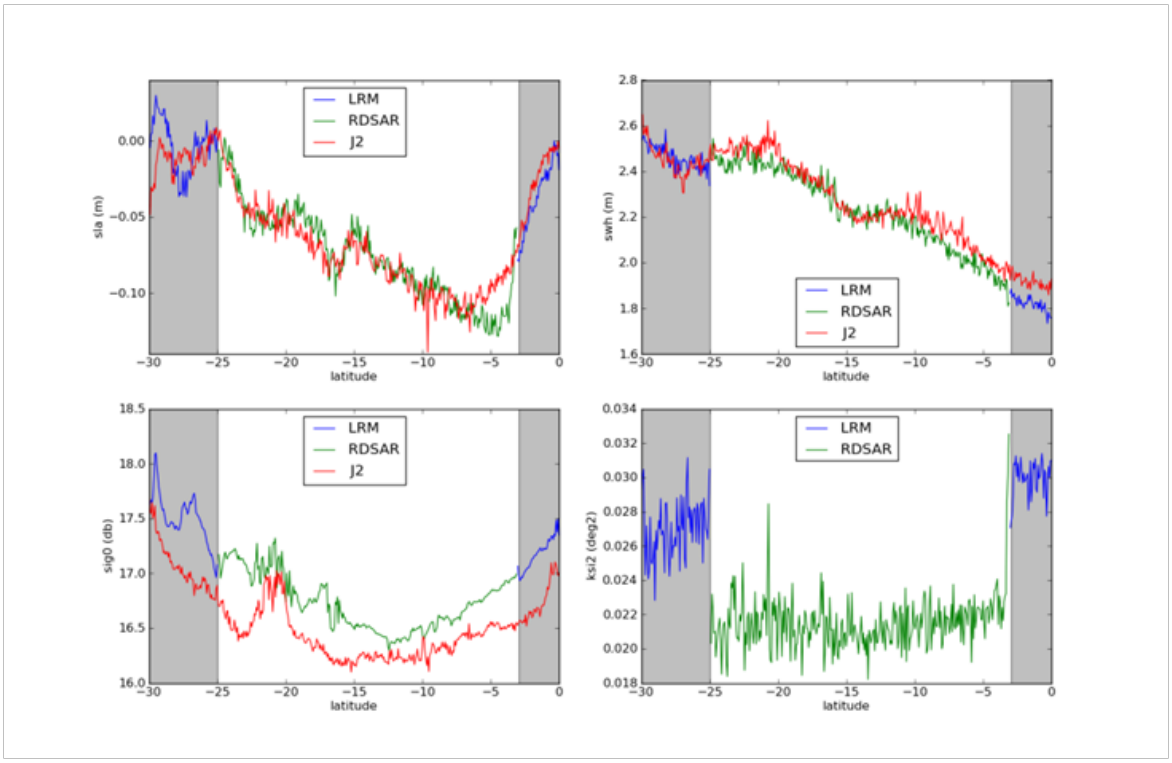

Figure 3.7: Mean of SLA (upper left), SWH (upper right), Sigma0 (lower left) and mispointing angles (lower right) by band of latitude for LRM and RDSAR of CryoSat-2 and LRM ofJason-2 - from 7th to 12th of May. The dashed zone corresponds to the LRM mode area.

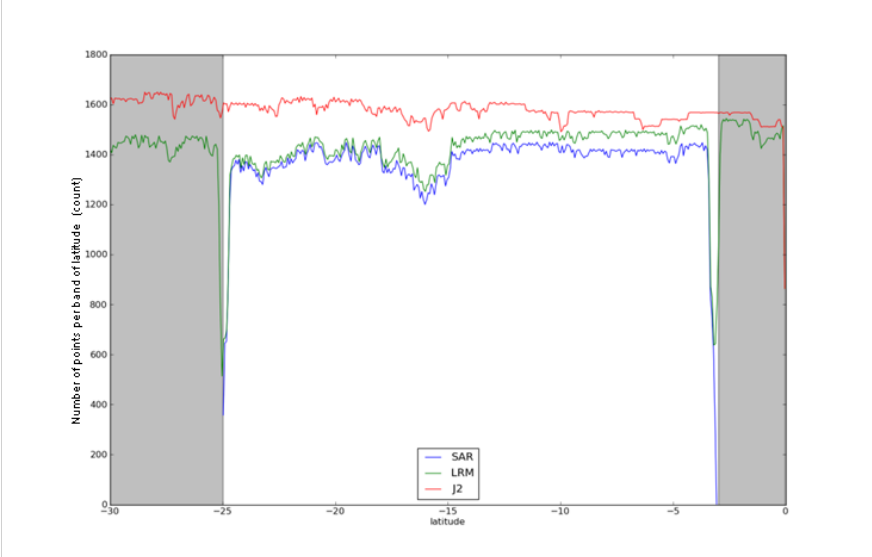

Figure 3.8: Density of points per band of latitude for LRM and RDSAR (and SAR) of CryoSat-2 mission and LRM of Jason-2 - from 15th to 25th of May.

4. Conclusion

The continuity assessment between LRM and RDSAR data has been performed in open ocean in the equatorial Pacific test area. Results show in general a very good agreement at the transition, with no significant bias in SLA and SWH in both modes. Additionally the 1Hz noise on SLA/SWH RDSAR data is higher than the LRM one as expected, but a better RDSAR data precision is obtained (than the sqrt(3) factor) since in reality more pulses contribute to the pulse de-correlation than what is suggested in theory.

Biases found at the continuity between RDSAR estimates and LRM ones are no significant. These biases are likely of approximate size of the errors of estimates due to the noisier RDSAR measurements. The speckle reduction performance of the reduced SAR approach is not as efficient as for the conventional altimeter pulse-limited resolution mode. Due to this higher measurement noise, the RDSAR echo shape is slightly different to the LRM one, leading to discrepancies in the way the model fits the echo over identical sea state. Appropriate look-up tables will be computed to take into account this effect and correct the estimations (range, significant waveheight, sigma0 and mispoiting angle) issued from an ocean analytical retracking algorithm.

We have demonstrated that the CPP reduced SAR L2 products are a good LRM-reference during SAR-mode maintaining the continuity with the LRM mode data and then allowing the assessment of the in-orbit performances of the SAR mode data.

5. References

[Amarouche et al., 2004]: L. Amarouche, P. Thibaut, O.Z. Zanife, J.-P. Dumont, P. Vincent and N. Steunou, "*Improving the Jason-1 ground retracking to better account for attitude effects*", marine Geodesy, Vol. 27, pp.171-197, 2004.